ADVANCED FUNCTIONAL MATERIALS
www.afm-journal.de

Flexible and Transparent Nanocomposite of Reduced Graphene Oxide and P(VDF-TrFE) Copolymer for High Thermal Responsivity in a Field-Effect Transistor

*Tran Quang Trung, Subramanian Ramasundaram, Seok Won Hong, and Nae-Eung Lee**

A new class of temperature-sensing materials is demonstrated along with their integration into transparent and flexible field-effect transistor (FET) temperature sensors with high thermal responsivity, stability, and reproducibility. The novelty of this particular type of temperature sensor is the incorporation of an R-GO/P(VDF-TrFE) nanocomposite channel as a sensing layer that is highly responsive to temperature, and is optically transparent and mechanically flexible. Furthermore, the nanocomposite sensing layer is easily coated onto flexible substrates for the fabrication of transparent and flexible FETs using a simple spin-coating method. The transparent and flexible nanocomposite FETs are capable of detecting an extremely small temperature change as small as 0.1 °C and are highly responsive to human body temperature. Temperature responsivity and optical transmittance of transparent nanocomposite FETs were adjustable and tuneable by changing the thickness and R-GO concentration of the nanocomposite.

1. Introduction

Physical sensing devices are promising in various applications including personal health monitoring, electronic skins, robot sensors, and other human-machine interface systems.[1–17] Physical sensing devices have been designed for increased convenience in real-life applications and include multi-functional features such as transparency, flexibility and stretchability.[1–4,6–9,11–16] Among these, temperature sensors that are mechanically flexible, light-weight, inexpensive, and easily attached to a substrate will play an important role in detecting human body temperature and in monitoring perishable food, electronic skins, and in other environmental monitoring applications.[3,11,15,18] The optical transparency of the flexible temperature sensor may enable its easy integration into human-friendly, flexible and transparent electronics. Several types of flexible temperature sensors such as thermocouples[19] and resistive temperature detectors[15] have been developed. Recently, a resistive flexible Ni composite-based temperature sensor developed by Bao et al.[18] showed a small dynamic range (25 to 40 °C). Rogers et al.[15] introduced a class of stretchable temperature sensors based on the temperature coefficient resistance (TCR) using serpentine gold and a PIN diode using Si nanoribbons transferred onto microperforated elastomers, which can monitor precise and continuous thermal characterization of human skin. These temperature sensors are not optically transparent because conventional opaque inorganic sensing materials and electrodes were used. Therefore, the development of a flexible temperature sensor with high responsivity, transparency, ease of integration, large dynamic range, and stability in an ambient environment is an alternative, suitable approach for realizing the stable monitoring of temperature in many flexible and transparent electronic systems.

Graphene (Gr) has exceptional electrical and mechanical properties and has shown interesting stimuli-responsive properties to light,[20–22] heat,[23,24] and strain.[12,25,26] In addition, graphene and reduced graphene oxide (R-GO) are also known as multi-functional materials with transparency, flexibility, and stretchability.[27–34] Based on those features, Gr or R-GO is a promising candidate as a physically responsive material for sensing devices. There have been recent reports regarding different types of physically responsive FETs (physi-FETs) for sensing applications based on Gr and R-GO. These include, for example, photodetectors based on mechanically exfoliated Gr and Gr nanoribbons,[20,21] phototransistors from band gap-tuneable R-GO,[35] thermal sensors based on a networked R-GO,[24] and strain sensors based on Gr and R-GO.[12,25] Although these physical sensing devices make possible new fields of applications in electronics, the many processing steps required, such

Dr. T. Q. Trung, Prof. N.-E. Lee
School of Advanced Materials Science & Engineering
Sungkyunkwan University (SKKU)
Suwon, Kyunggi 440–746, Korea
E-mail: nelee@skku.edu
Dr. S. Ramasundaram, Dr. S. W. Hong
Center for Water Resource Cycle Research
Korea Institute of Science and Technology
Hwarangno 14 gil
Seongbuk-gu, Seoul 136–791, Korea
Prof. N.-E. Lee
SKKU Advanced Institute of Nanotechnology (SAINT), SKKU
Suwon, Kyunggi 440–746, Korea
Prof. N.-E. Lee
Samsung Advanced Institute for Health Sciences & Technology (SAIHST),SKKU
Suwon, Kyunggi 440–746, Korea

DOI: 10.1002/adfm.201304224

as mechanical exfoliation of Gr,[36] and formation of a thin continuous R-GO network[12,24,37,38] for integration into the FET structure make their fabrication complex, costly, of low yield, and difficult to control. In addition, without encapsulation, the Gr and R-GO channels are highly susceptible to ambient molecular species which will cause instability in the electrical properties of the sensing device. Therefore, the use Gr or R-GO alone did not minimize the problem of stability of physi-FETs to environmental effects.[24,39,40] Hence, development of a physical sensing material-based R-GO that can be incorporated into FETs with a simple process, reinforced responsivity to physical stimuli, and improved stability in ambient conditions is needed to develop a high performance physi-FET based on nano carbon materials.

Herein, a transparent and flexible temperature sensor was developed using an FET structure that has a temperature-responsive layer of R-GO/P(VDF-TrFE) nanocomposite as a channel. The key component of this device is the sensing layer of the R-GO/P(VDF-TrFE) nanocomposite, which is highly responsive to temperature and is optically transparent and mechanically flexible. Furthermore, the sensing layer of the R-GO/P(VDF-TrFE) nanocomposite is easily coated onto a large-area substrate for the fabrication of transparent and flexible devices using a simple spin-coating method. The total amount of R-GO in an R-GO/P(VDF-TrFE) nanocomposite can be controlled by adjusting the layer thickness or R-GO concentration in R-GO/P(VDF-TrFE) nanocomposites for enforced responsivity to temperature stimuli. The temperature response of the transparent and flexible nanocomposite FETs was examined by measuring at two different temperature ranges, at intervals of 1 °C over a small range (30 to 40 °C) and at intervals of 5 °C at a large range (30 to 80 °C).The transparent and flexible nanocomposite FET was able to detect an extremely small temperature change as small as 0.1 °C and was highly responsive to the temperature of the human body. The temperature sensor exhibited high thermal responsivity, stability, and reproducibility under ambient conditions. Temperature responsivity and optical transmittance of the transparent nanocomposite FET were adjustable and tuneable by changing the thickness and R-GO concentration of the nanocomposite. The hydrophobic P(VDF-TrFE) matrix minimized the environmental effects caused by polar solvents, moisture, or water vapor on the sensing capability under ambient conditions, which enabled the fabrication of highly stable, sensitive, flexible and transparent thermal FET sensors.

2. Results and Discussion

To integrate R-GO/P(VDF-TrFE) nanocomposite thin film as a channel in an FET structure of a temperature sensor, R-GO/P(VDF-TrFE) nanocomposite thin films were fabricated with varying thickness (90, 128, and 204 nm) and R-GO concentration (8, 10, and 12 wt%). The details of material preparation and device fabrication are presented in the Experimental Section. The nanocomposite thin films were electrically conductive with a sheet resistance on the order of 0.521 to 18.9 MΩ/□, depending on the thickness and R-GO concentration of the R-GO/P(VDF-TrFE) nanocomposite thin films. The size of

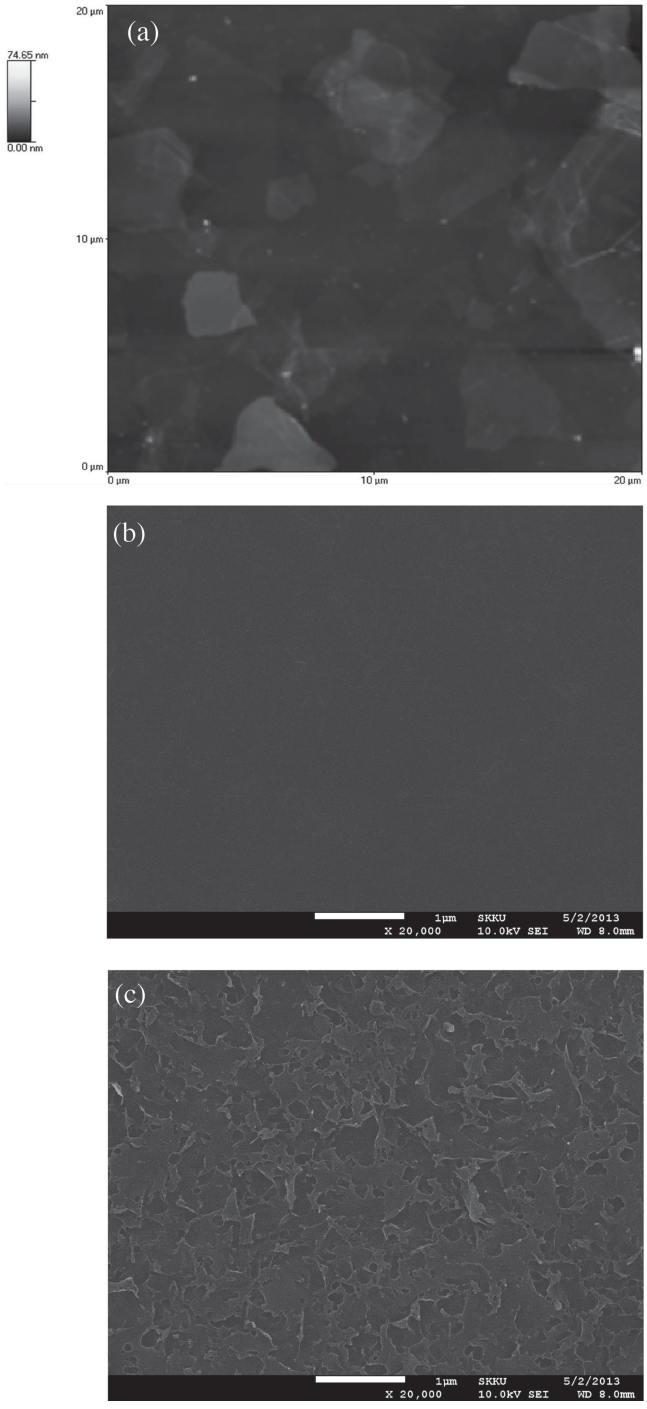

Figure 1. (a) AFM image of the R-GO/P(VDF-TrFE) nanocomposite with an R-GO concentration of 10 wt%. FE-SEM images of the R-GO/P(VDF-TrFE) nanocomposite with an R-GO concentration of 10 wt% (b) without and (c) with an O_2 chemical dry etching (CDE) process.

the R-GO nanosheet and surface morphology of the R-GO/P(VDF-TrFE) nanocomposite thin film with an R-GO concentration of 10 wt% were confirmed by atomic force microscopy (AFM). **Figure 1**a shows an AFM image of R-GO nanosheets at the nanocomposite surface. The average size of the R-GO nanosheet was around 2 to 3 μm, and most of the R-GO

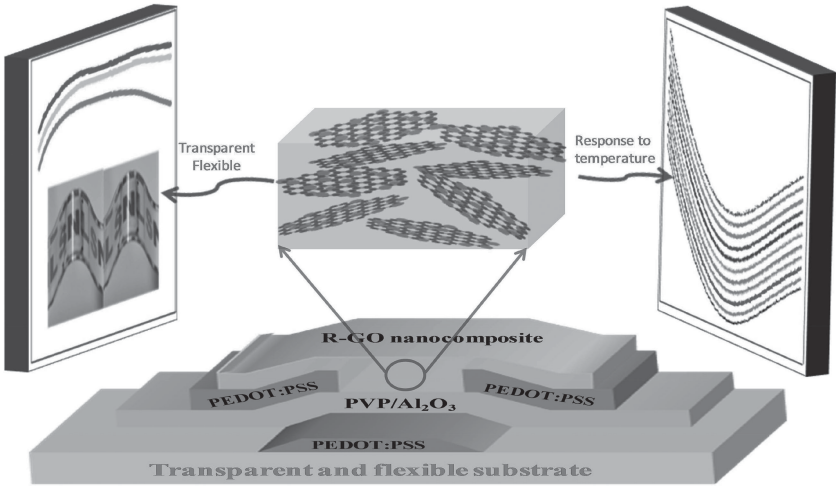

Figure 2. Schematic of transparent, flexible R-GO/P(VDF-TrFE) nanocomposite FET. The schematic illustrates structural, optical (transparent) and electrical (response to temperature) properties of the transparent, flexible R-GO/P(VDF-TrFE) nanocomposite FET.

nanosheets were aligned nearly parallel to the substrate surface. In nanocomposite materials, the electrical transport mechanism is governed by distribution of the filler material in the matrix polymer.[41] To further examine the distribution of R-GO nanosheets within the polymer matrix P(VDF-TrFE), the surface of the R-GO/P(VDF-TrFE) nanocomposite thin film with an R-GO concentration of 10 wt% was etched by an O_2 chemical dry etching (CDE) process to remove surface of P(VDF-TrFE) and expose the R-GO nanosheet network within the polymer matrix. After CDE, the sample was observed by field-emission scanning electron microscopy (FE-SEM). Figures 1b and c show FE-SEM images of the R-GO/P(VDF-TrFE) nanocomposite with and without the CDE process, respectively. In the case of the film with no CDE process (Figure 1b), it was not possible to observe the R-GO distribution within the polymer matrix because the R-GO nanosheets were almost completely buried in the P(VDF-TrFE) polymer matrix. After differential removal of the P(VDF-TrFE) by an O_2 CDE process, a network of R-GO nanosheets within the polymer matrix was observed (Figure 1c). The results demonstrate that this nanocomposite preparation process produces highly dense R-GO nanosheets that are well distributed within the polymer matrix P(VDF-TrFE), and R-GO nanosheets in P(VDF-TrFE) were expected to have a larger contact area between neighboring R-GO nanosheets rather than having end to end connections in networked R-GO.

The transparent nanocomposite FETs were fabricated in bottom-gate and bottom-contact configuration on both glass and flexible substrates for evaluation of their fundamental properties. To determine the transparency of the device, the gate, source, and drain electrodes of the device were made from a conductive polymer poly(3,4-ethylenedioxythiophene) poly(4-styrenesulfonate) (PEDOT:PSS) by spin-coating and patterning using dry etching. In this paper, we first fabricated transparent nanocomposite FETs on glass substrates to investigate the effects of nanocomposite thickness and R-GO concentration on the optical transmittance, electrical characteristics, and response to the temperature of the fabricated devices. To demonstrate the capability of applications in transparent flexible electronics, a nanocomposite FET temperature sensor with mechanical flexibility, low weight, and ease of attachment was fabricated on a flexible poly(ether sulfones) (PES) substrate. **Figure 2** shows a schematic of the device structure, which is flexible and transparent in the visible range and has the capability of temperature response.

Before using the device in temperature sensing applications, we first investigated the effects of the thickness of R-GO/P(VDF-TrFE) nanocomposite on the electrical properties and transmittance of the transparent nanocomposite FET. Transfer characteristics of the transparent R-GO/P(VDF-TrFE) (8 wt% R-GO) nanocomposite FET with various R-GO composite thicknesses (204, 128, and 90 nm) were ambipolar (Supporting Figures S1a,b,c). That is, both electron and hole currents can be induced by gate voltage (V_G) biasing. To confirm the optical transmittance of devices, the total optical transmission spectra were measured through the stacked blanket layers on a glass substrate that had the same thickness as those of the layers in the transparent nanocomposite FET structure. As shown in the results presented in Supporting Figure S1d, the optical transmission of the glass substrate with stacked blanket layers in the visible wavelength ranging from 350 to 800 nm was about 55% to 65% depending on the thickness of the R-GO composite. The optical images of the nanocomposite FETs with different R-GO composite thicknesses (see the inset in Supporting Figure S1d) show optical transparency, in which the text on the paper behind the substrate of the devices is clearly visible.

The response of transparent nanocomposite FET to temperature was investigated by measuring the transfer characteristics of devices over a temperature range from 30 to 80 °C. The typical response of source-drain current (I_{DS}) is plotted in **Figure 3**a. The I_{DS} extracted from the transfer curves in Figure 3a are presented as a function of temperature in Figure 3b. In addition, to elucidate the response of transparent nanocomposite FET to temperature variation, the device was measured over a smaller temperature range of 30 to 40 °C at an interval of 1 °C (Supporting Figures S2a,b). The I_{DS} or conductivity increased as temperature increased, suggesting a semiconducting behavior of the R-GO nanocomposite. This phenomenon is attributed to the fact that R-GO nanosheets in P(VDF-TrFE) have a larger contact area between neighboring R-GO nanosheets rather than having end to end connections in networked R-GO. Therefore, the temperature dependence of the conductivity of the R-GO/P(VDF-TrFE) nanocomposite can be suggested to occur by two main mechanisms: the hopping transport mechanism and a tunneling conduction mechanism.[23,24,42] Careful examination of the transfer curves in Supporting Figure S3 reveals changes in the slope with respect to temperature, which indicates the contribution of the charge transport mechanism between adjacent R-GO nanosheets within the P(VDF-TrFE) matrix. Therefore, complete understanding of the temperature sensing mechanism in a transparent nanocomposite FET requires investigation of the tem-

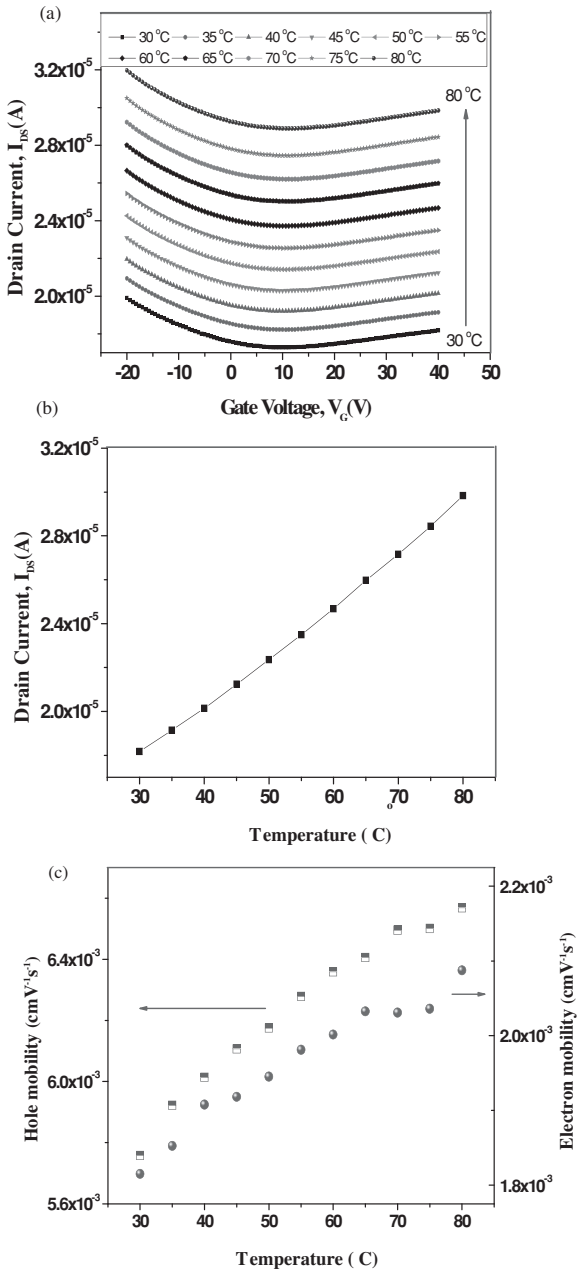

Figure 3. (a) The transfer characteristics of the R-GO/P(VDF-TrFE) nanocomposite FET were measured over a large range temperature, 30 to 80 °C, with a temperature interval of 5 °C. (b) The I_{DS} was extracted from transfer characteristics at V_{DS} = 15 V and V_G = 40 V as a function of temperature over a large temperature range. (c) The electron and hole field-effect mobilities extracted from the transfer characteristics (Figure 3a) as a function of temperature showed increasing trends as the temperature increased.

perature dependence of field-effect carrier mobility, μ. The hole and electron field-effect mobilities shown in Figure 3c gradually increased with increasing temperature from 30 to 80 °C, which can be explained by the hopping transport of charge carriers in the R-GO/P(VDF-TrFE) nanocomposite. For connected R-GO nanosheets in the P(VDF-TrFE) matrix thin film, the presence of defects and disorders localized or trapped the carrier travel near the potential barriers. If the carrier becomes localized at a defect, then lattice vibrations are essential if the carrier is to move from one site to another.[24] This is a hopping transport process, and the field-effect mobilities are expected to increase with increasing temperature.

For investigation of effects of the thickness and R-GO concentration on temperature responsivity of transparent nanocomposite FET, we fabricated devices using R-GO/P(VDF-TrFE) nanocomposite with an R-GO concentration of 8 wt% with varying thickness (90, 128, and 204 nm) and also used a 200-nm-thick nanocomposite with varying R-GO concentration (8, 10, 12, and 17 wt%). Response characteristics of the devices to temperature were systematically measured. The temperature response of devices with different thickness and R-GO concentration are presented in **Figure 4**a and b, respectively. The increased responsivity with respect to increasing the thickness (Supporting Figure S4a) and R-GO concentration (Supporting Figure 4b) demonstrate that the sensing capability of transparent nanocomposite FET strongly depends on the characteristics of the sensing layer of the R-GO/P(VDF-TrFE) nanocomposite. By controlling the thickness of nanocomposite and the amount of R-GO nanosheets in the matrix polymer, the responsivity of the nanocomposite to stimuli (temperature) is tuneable. Therefore, the responsivity of R-GO/P(VDF-TrFE) nanocomposite will increase with increases in thickness and R-GO concentration. However, with increased thickness and amount of R-GO nanocomposite, the optical transmittance decreased (see Supporting Figures S1d and S6). For optimization of a transparent nanocomposite FET for thermal sensing, therefore, we must control the thickness and R-GO amount in the nanocomposite to balance the optical transmittance and thermal responsivity of the devices. In addition, the V_G effect on the responsivity of devices was also investigated. The device with an R-GO concentration of 8 wt% and nanocomposite thickness of 204 nm was measured to obtain its response characteristics with regard to temperature under no gate bias and various negative V_g values (–10 to –30 V). Figures 4c showed the temperature response of devices with different V_g. The increased responsivity (Supporting Figure S4c) with increasing negative V_g resulted in an increase of hole current under negative V_G.

In order to confirm the repeatability of the devices with the same nanocomposite channel, seven devices with the same nanocomposite with an R-GO concentration of 8 wt% and thickness of 200 nm were fabricated and characterized. As seen in Supporting Figures S5a and 5b, the device-to-device variation in the $I_{min,DS}$ response to temperature and the responsivity was measured to be $1.597 \times 10^{-5} \pm 1.220 \times 10^{-6}$ (A) and $2.483 \times 10^{-7} \pm 7.209 \times 10^{-9}$ (A/°C), respectively. However, the difference in sensing characteristics of the devices was not significant. With a proper calibration procedure, the device can be applied to temperature sensing.

As aforementioned, stability and reproducibility in sensing applications of physi-FETs are of critical importance. Therefore, for additional evaluation of reliability in the temperature response of transparent nanocomposite FETs, the stability and reproducibility of the device with R-GO concentration of 8 wt% and thickness of 204 nm at ambient conditions were evaluated. The electrical stability of the transparent nanocomposite FETs was examined by 12 repeated measurements with an interval

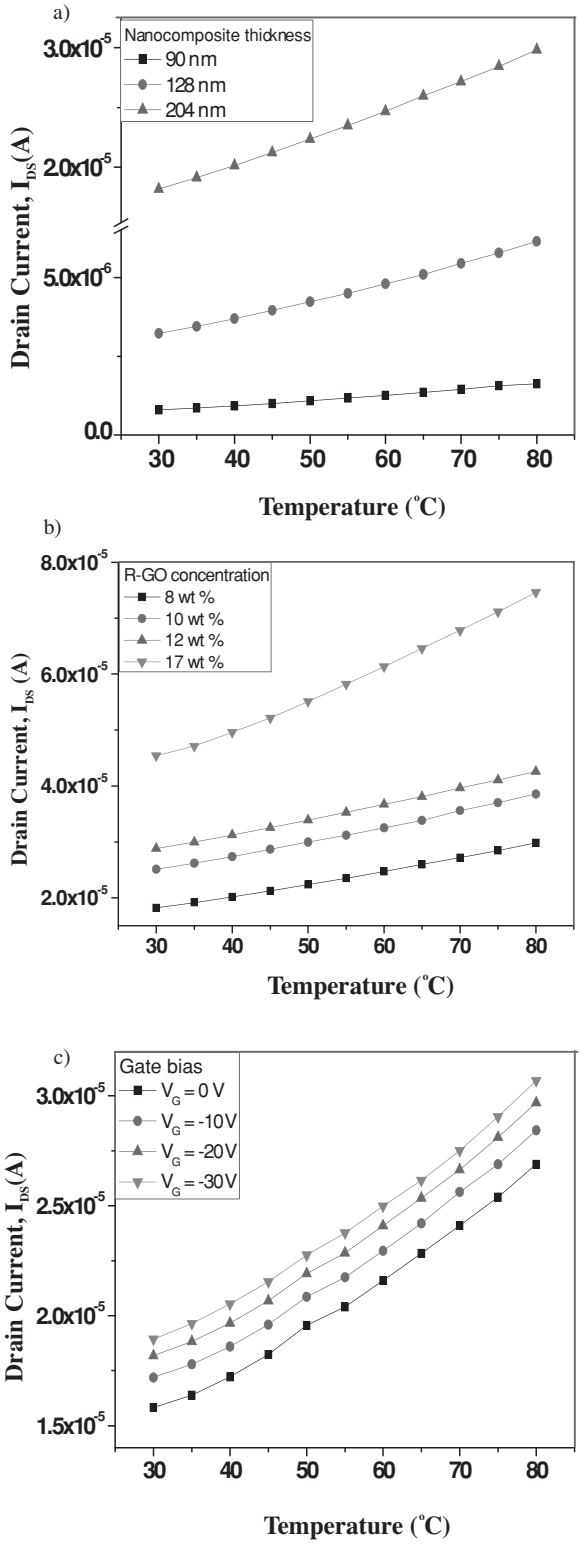

Figure 4. (a) I_{DS} response of the transparent nanocomposite FET to temperature at different thicknesses of nanocomposite measured at V_{DS} = 15 V and V_G = 40 V. (b) I_{DS} response of the transparent nanocomposite FET to temperature at different concentrations of R-GO nanocomposite measured at V_{DS} = 15 V and V_G = 40 V. (c) I_{DS} response of the transparent nanocomposite FET to temperature measured at V_{DS} = 15 V and gate bias voltages of V_G = 0, −10, −20, and −30 V.

time of 1 hr in ambient conditions. Supporting Figures S7a,b present the nearly unchanged transfer characteristics and charge neutrality point (CNP) of the device after exposure to air for 12 hr, respectively. Based on this measurement, it can be concluded that the transparent nanocomposite FET with R-GO dispersion in hydrophobic copolymer, (P(VDF-TrFE)), matrix is resistant to electrical instability caused by oxygen, moisture, or water molecules in ambient conditions. In this case, the hydrophobic copolymer P(VDF-TrFE) serves as a barrier that prevents the absorption of oxygen, moisture, or water molecules on R-GO nanosheets dispersed in a hydrophobic copolymer (P(VDF-TrFE)) matrix. Changes in the reproducibility of the devices were examined by measuring the device under cyclic heating. The temperature response of the devices was measured during three heating cycles over a temperature range of 30 to 80 °C with an interval of 5 °C, and the response values of minimum current ($I_{DS,min}$) were recorded for each heating cycle. The response values of $I_{DS,min}$ for individual heating cycles indicated good reproducibility of the device signal during three heating cycles (Supporting Figure S8). However, there was a small difference in $I_{DS,min}$ in response to the heating and cooling cycles, which can be attributed to the slight hysteresis in the temperature response of the R-GO/P(VDF-TrFE) nanocomposite. Based on these results, it can be concluded that the transparent nanocomposite FETs are highly reproducible in response to temperature change.

To demonstrate a temperature sensor with mechanically flexibility that is light weight and easily attached to a substrate, transparent and flexible nanocomposite FETs on flexible PES substrate were fabricated. **Figure 5**a presents ambipolar transfer characteristics of transparent and flexible nanocomposite FET with R-GO concentration of 12 wt% and thickness of 250 nm. The transparent flexible device showed slightly lower electron and hole field-effect mobility values compared to the device fabricated on a glass substrate (see Supporting Table S1). These results are attributed to the difference in the thickness and materials of gate dielectric layer employed in the devices on the flexible and glass substrates. In the case of the device on the flexible substrate, the flexible hybrid organic-inorganic (Al_2O_3 (20 nm)/PVP (400 nm)/Al_2O_3 (20 nm)) dielectric layer is used,[43,44] which has greater thickness and lower capacitance than the dielectric layer (Al_2O_3 (200 nm)) of the device on a glass substrate. Thus, the amount of induced charges at the interface between the gate dielectric and R-GO/P(VDF-TrFE) nanocomposite in the flexible device is lower than in the rigid device, which results in a lower gate effect, leading to a lower field-effect mobility of the charge carrier in the flexible device. The optical image of the transparent and flexible nanocomposite FET (see the inset in Figure 5a) indicates optical transparency, in which the text on the paper behind the substrate with the devices is clearly visible. The response of transparent, flexible nanocomposite FET to temperature was investigated by measuring the transfer characteristics of the devices over a temperature range from 30 to 80 °C, and the typical response of the I_{DS} is plotted in Supporting Figure S9a. The I_{DS} values extracted from the transfer curves in Supporting Figure S9a are presented as a function of temperature in Supporting Figure S9a. Response behaviors of the flexible device to temperature showed the same tendencies as those of the rigid device on glass substrate.

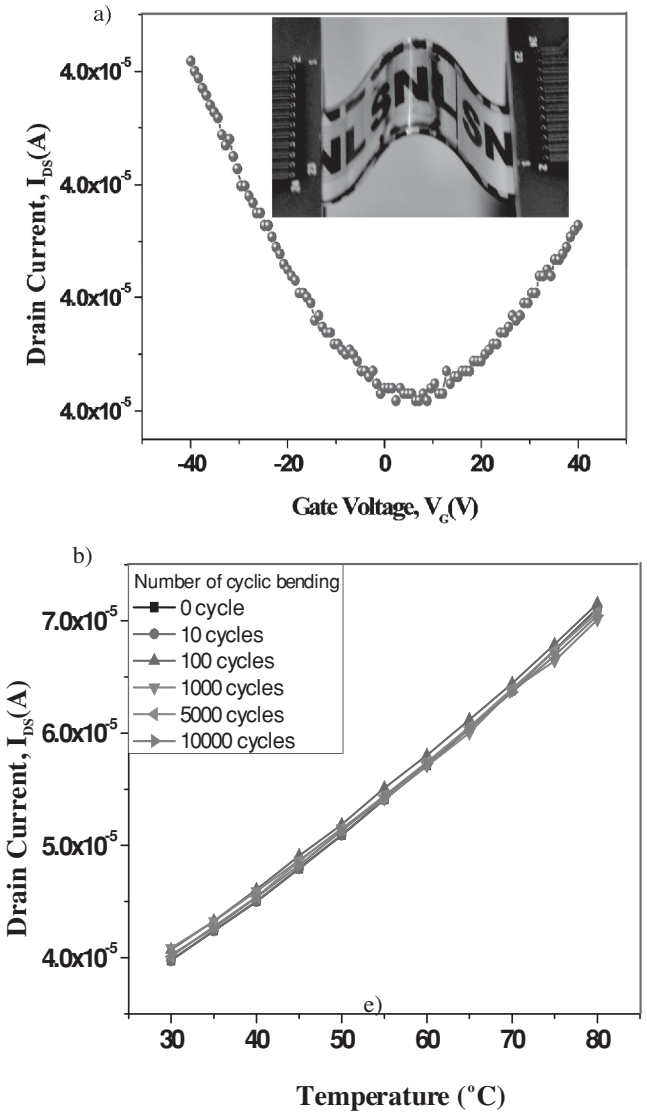

Figure 5. (a) Transfer characteristics of a transparent and flexible nanocomposite FET. The inset shows the optical image of the transparent, flexible FET loaded onto an electrical measurement system with the capability of cyclic bending. (b) The I_{DS} response of the transparent, flexible nanocomposite FET to temperature after cyclic bending.

In addition, to evaluate the reliability of the transparent, flexible nanocomposite FETs after repetitive mechanical deformations, the sensing capability and responsivity of the device were evaluated after cyclic bending of the devices. The temperature response and responsivity of the devices being subjected to10, 100, 1,000, 5,000, and 10,000 bending cycles at the strain of 0.3% are presented in Figure 5b and Supporting Figure S9c, respectively. The response characteristics of the device to temperature are nearly unchanged, and there is a slight decrease in responsivity after more than 1,000 bending cycles (see Supporting Figure S9c). From these results, it can be presumed that the sensing capability of the transparent, flexible nanocomposite FET after cyclic bending is relatively stable.

Interestingly, the transparent, flexible nanocomposite FET has the ability to detect an extremely small temperature change, as small as 0.1 °C, and is highly responsive to the temperature of the human body. Based on these features, the temperature sensor appears promising in the precise thermometry of human skin for use in the provision of relevant information about personal health. To investigate the response of the device to extremely small changes in temperature, the transfer characteristics of the devices were measured over a temperature range of 31 to 32 °C at intervals of 0.1 °C, and the typical response of I_{DS} is plotted in **Figure 6**a. The I_{DS} values extracted from the transfer curves in Figure 6a are presented as a function of temperature in Figure 6b. In addition, to demonstrate the potential application of the transparent, flexible nanocomposite FET in personal health monitoring, we examined the sensing capability of the device for temperature measurements of the human body. For this purpose, a transparent, flexible nanocomposite FET was attached to a human hand (see Figure 6d). The temperature of the sensor was calibrated as follows: (i) a minimum current response to temperature of human body ($I_{DS,min}^{body} = 3.7689 \times 10^{-5}$ (A) was recorded, (ii) a minimum source-drain current ($I_{DS,\,min}$) was established for the device as function of temperature (T) (see Figure 6c) by measuring the transfer characteristics of the device from 30 to 80 °C at intervals of 1 °C (see Supporting Figure S10), and (iii) body temperature was interpolated from the value of $I_{DS,min}^{body}$ and as a function of $I_{DS,\,min}$ versus temperature. Figure 6c showed that the response of $I_{DS,\,min}$ to temperature was fitted as two linear functions of temperature. The first linear function was d_1: $I_{DS,\,min} = 5.13415 \times 10^{-7}\,T + 1.89054 \times 10^{-5}$ corresponding at a low temperature range (30–52 °C), and the second linear function was d_2: $I_{DS,\,min} = 6.00628 \times 10^{-7}\,T + 1.43858 \times 10^{-5}$ corresponding to a high temperature range (52–80 °C). We realized that the $I_{DS,min}^{body} = 3.7689 \times 10^{-5}$ (A) belonged to the first linear function, d_1. Therefore, the temperature of the human body was calibrated by substituting $I_{DS,min}^{body}$ into equation d_1. Measured body temperature was 36.6 °C. (see Figure 6c). For additional evaluation of the reliability of the response to body temperature in transparent, flexible nanocomposite FETs, the temperature sensor was attached to a human hand on three occasions, and response values of $I_{DS,min}^{body} = 3.7689 \times 10^{-5}$, 3.7694×10^{-5}, and 3.7789×10^{-5} (A) were recorded for each measurement. By substituting $I_{DS,min}^{body}$ into equation d_1, we obtained body temperature measurements that corresponded to 36.6, 36.6, and 36.8 °C (see Supporting Figure S11).These results demonstrate that the transparent, flexible nanocomposite FET can deliver accurate measurements of human body temperature.

3. Conclusions

In this work, a new class of FET thermal sensor was developed based on a transparent, flexible, highly sensitive, and solution-processable R-GO/P(VDF-TrFE) nanocomposite. Using the new thermal sensing material, which was synthesized as a nanocomposite of R-GO and hydrophobic polymer (P(VDF-TrFE)) in an FET structure, a thermal sensing device with high responsivity and excellent stability and reproducibility was developed. Use of hydrophobic P(VDF-TrFE) as a polymer matrix improved the stability and reproducibility of the devices in ambient conditions. The hopping and tunneling

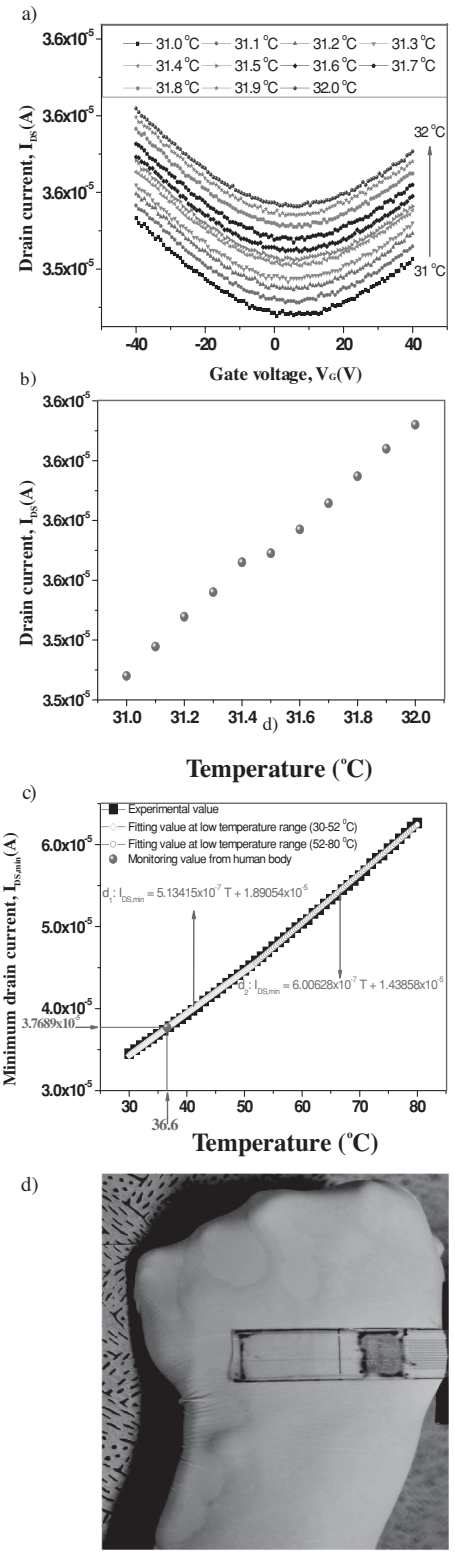

Figure 6. (a) Transfer characteristics of transparent, flexible nanocomposite FETs were measured over an extremely small temperature range, 31 to 32 °C, using a temperature interval of 0.1 °C. (c) The I_{DS} at V_{DS} = 15 V and V_G = 40 V was extracted from the transfer characteristics (Figure 6a) as a function of temperature. (c) The response of $I_{DS, min}$ to temperature was fitted as two linear functions of temperature. The first linear function was d_1: $I_{DS, min} = 5.13415 \times 10^{-7} T + 1.89054 \times 10^{-5}$ corresponding to the small temperature range (30–52 °C), and the second linear function was d_2: $I_{DS, min} = 6.00628 \times 10^{-7} T + 1.43858 \times 10^{-5}$ corresponding to the large temperature range (52–80 °C). The temperature of the human body was calibrated by substituting $I^{body}_{DS,min} = 3.7689 \times 10^{-5}$ into equation d_1. A body temperature of 36.6 °C was obtained. (d) The picture illustrates the measurement process of response values of $I^{body}_{DS,min}$ to human body temperature.

transport within R-GO/P(VDF-TrFE) were used to explain the thermal sensing mechanism of the transparent R-GO/P(VDF-TrFE) nanocomposite FET by analyzing the transfer characteristics. The increased R-GO amount in the R-GO/P(VDF-TrFE) nanocomposite and its greater thickness enhanced the responsivity to thermal load. The highly responsive features of the transparent, flexible nanocomposite FET offer great promise in fields of transparent flexible electronics or monitoring temperature of the human body and as an electronic skin and human-machine interface.

4. Experimental Section

Preparation of Functional Graphene Oxide: To facilitate the dispersion of graphene oxide (GO) in the polar aprotic solvent, *N,N'*-dimethylacetamide (DMAC), the carboxyl and hydroxyl groups were derivatized with amide and carbamate ester groups by contacting graphite oxide with phenylisocyanate. GO nanosheets were prepared by modified Hummer's methods.[45] The derivatization of GO was performed using the procedure reported by Stankovich et al.[46] In brief, the saturated suspension of graphite oxide was prepared by stirring 500 mg of graphite oxide with 50 mL of *N,N'*–dimethylformamide (DMF) for 5 h. Then 20 mM (2.3826 g) of phenylisocyanate was added and stirred under a nitrogen atmosphere for 24 h. The reaction mixture was coagulated by addition into 500 mL of methylene chloride. The solvent was removed by filtration after precipitation. The precipitate was further washed twice with 500 ml methylene chloride and dried overnight at ambient temperature to obtain graphite oxide with amide and carbamate esters. Functionalized GO nanosheet dispersion with a solid content of 2.5 mg were obtained by sonicating with phenylisocyanate-treated graphite oxide with DMAC.

Fabrication of R-GO/P(VDF-TrFE) Composite Thin Films: In this paper, the liquid phase blending method was used to prepare all R-GO/P(VDF-TrFE) nanocomposite thin films. P(VDF-TrFE) was dissolved in DMAC with a concentration 0.1 g/mL. GO nanosheets dispersed in DMAC at a concentration of 2.5 mg/mL were mixed with appropriate weight fractions of P(VDF-TrFE) solution and stirred for 12 h before being sonicated for 10 min at room temperature. The GO nanosheets in the P(VDF-TrFE) matrix were reduced by a two-step in-situ reduction technique, which consisted of a phenylhydrazine reduction (2 μL hydrazine per 1 mL of dispersed GO in DMAC with a concentration 5 mg/mL) and a subsequent thermal reduction at 150 °C for 4 h under vacuum. For use of a nanocomposite material as a channel layer in the FET, the R-GO/P(VDF-TrFE) nanocomposite thin film with 8, 10, and 12 wt.% loading of R-GO was fabricated by the spin-coating method.

Fabrication of Transparent R-GO/P(VDF-TrFE) Composite FET: Transparent R-GO/P(VDF-TrFE) nanocomposite FET devices were fabricated in a bottom-gate and bottom-contact configuration on both flexible and glass substrates. The spin-coated poly(3,4-ethylenedioxythiophene) poly(4-styrenesulfonate) (PEDOT:PSS), which was used as the gate, source and drain electrodes, was patterned by an O_2 CDE (chemical dry etching) process. After the spin-coating of PEDOT:PSS on both the poly(ether sulfones) (PES) (transparent and flexible device) and glass substrates (transparent device), a thin film of Ni (5 nm) was deposited as an etch mask through a shadow mask onto

the PEDOT:PSS film by e-beam evaporation. Then, the substrate was exposed to an oxygen microwave plasma in a CDE system at 640 mTorr and a microwave power of 50 W to etch the PEDOT:PSS not protected by the Ni patterns. Finally, the Ni mask patterns were removed in an HNO_3 acid solution. With this patterning technique, transparent R-GO/P(VDF-TrFE) composite FET with channel lengths ranging from 40 to 70 μm and a channel width of 800 μm were obtained. For the device on glass substrate, a 200-nm-thick Al_2O_3 gate dielectric layer was deposited by atomic layer deposition (ALD) at 200 °C. Finally, a R-GO/P(VDF-TrFE) nanocomposite channel layer with various R-GO concentrations (8, 10, and 12 wt.%) and thicknesses (90, 128, and 204 nm) was spin-coated on the top of the source-drain electrodes. For the flexible device, the hybrid organic-inorganic (Al_2O_3 (20 nm)/PVP (400 nm)/Al_2O_3 (20 nm)) gate dielectric layer was used. A 20-nm-thick Al_2O_3 layer was deposited by ALD at 200 °C, and a 400-nm-thick PVP was deposited by the spin-coating method.

Supporting Information

Supporting Information is available from the Wiley Online Library or from the author.

Acknowledgements

T. Q. Trung and S. Ramasundaram contributed equally to this work. This research was supported by the Basic Science Research Program (Grant No. 2010–0015035 and 2013R1A2A1A01015232) through the National Research Foundation (NRF) funded by the Ministry of Science, ICT& Future Planning. This research was also supported by a grant from the Korea Ministry of the Environment as a "Converging Technology Project" (2012000600001).

Received: December 19, 2013
Published online: February 21, 2014

[1] S. C. B. Mannsfeld, B. C.-K. Tee, R. M. Stoltenberg, C. V. H.-H. Chen, S. Barman, B. V. O. Muir, A. N. Sokolov, C. Reese, Z. Bao, *Nat. Mater.* **2010**, *9*, 859.
[2] G. Schwartz, B. C.-K. Tee, J. Mei, A. L. Appleton, D. H. Kim, H. Wang, Z. Bao, *Nat. Commun.* **2013**, DOI: 10.1038/ncomms2832.
[3] T. Someya, Y. Kato, T. Sekitani, S. Iba, Y. Noguchi, Y. Murase, H. Kawaguchi, T. Sakurai, *Proc. Natl. Acad. Sci. USA* **2005**, *102*, 12321–12325.
[4] T. Q. Trung, N. T. Tien, Y. G. Seol, N.-E. Lee, *Org. Electron.* **2012**, *13*, 533–540.
[5] W. Wu, X. Wen, Z. L. Wang, *Science* **2013**, *340*, 952.
[6] C. Pang, G.-Y. Lee, T. Kim, S. M. Kim, H. N. Kim, S.-H. Ahn, K.-Y. Suh, *Nat. Mater.* **2012**, *11*, 795.
[7] K. Takei, T. Takahashi, J. C. Ho, H. Ko, A. G. Gillies, P. W. Leu, R. S. Fearing, A. Javey, *Nat. Mater.* **2010**, *9*, 821.
[8] D. J. Lipomi, M. Vosgueritchian, B. C.-K. Tee, S. L. Hellstrom, J. A. Lee, C. H. Fox, Z. Bao, *Nat. Nanotechnol.* **2011**, *6*, 788.
[9] T. Yamada, Y. Hayamizu, Y. Yamamoto, Y. Yomogida, A. Najafabadi, D. N. Futaba, K. Hata, *Nat. Nanotechnol.* **2011**, *6*, 296.
[10] J.-W. Jeong, W.-H. Yeo, A. Akhtar, J. J. S. Norton, Y.-J. Kwack, S. Li, S.-Y. Jung, Y. Su, W. Lee, J. Xia, H. Cheng, Y. Huang, W.-S. Choi, T. Bretl, J. A. Rogers, *Adv. Mater.* **2013**, DOI: 10.1002/adma.201301921.
[11] N. T. Tien, S. Jeon, D. Kim, T. Q. Trung, M. Jang, B.-U. Hwang, K.-E. Byun, J. Bae, E. Lee, J. B.-H. Tok, Z. Bao, N.-E. Lee, J.-J. Park, *Adv. Mater.* **2013**, DOI: 10.1002/adma.201302869.
[12] T. Q. Trung, N. T. Tien, D. Kim, M. Jang, O. J. Yoon, N.-E. Lee, *Adv. Funct. Mater.* **2013**, DOI: 10.1002/adfm.201301845.
[13] M. Kaltenbrunner, T. Sekitani, J. Reeder, T. Yokota, K. Kuribara, T. Tokuhara, M. Drack, R. Schwodiauer, I. Graz, S. B.-Gogonea, S. Bauer, T. Someya, *Nature* **2013**, *499*, 458.
[14] S. Bauer, *Nat. Mater.* **2013**, *12*, 871.
[15] R. C. Webb, A. P. Bonifas, A. Behnaz, Y. Zhang, K. J. Yu, H. Cheng, M. Shi, Z. Bian, Z. Liu, Y.-S. Kim, W.-H. Yeo, J. S. Park, J. Song, Y. Li, Y. Huang, A. M. Gorbach, J. A. Rogers, *Nat. Mater.* **2013**, DOI: 10.1038/NMAT3755.
[16] C. Wang, D. Hwang, Z. Yu, K. Takei, J. Park, T. Chen, B. Ma, A. Javey, *Nat. Mater.* **2013**, *12*, 899.
[17] M. L. Hammock, A. Chortos, B. C.-K. Tee, J. B.-H. Tok, Z. Bao, *Adv. Mater.* **2013**, *25*, 5997–6038.
[18] J. Jeon, H.-B.-R. Lee, Z. Bao, *Adv. Mater.* **2013**, *25*, 850–885.
[19] M. Imran, A. Bhattacharyya, *IEEE sens. J.* **2006**, *6*, 1459.
[20] F. Xia, T. Mueller, Y. Lin, A. V.- Garcia, P. Avouris, *Nat. Nanotech.* **2009**, *4*, 839.
[21] T. Mueller, F. Xia, P. Avouris, *Nat. Photo.* **2010**, *4*, 297.
[22] B. Chitara, L. S. Panchakarla, S. B. Krupanidhi, C. N. R. Rao, *Adv. Mater.* **2011**, *23*, 5419.
[23] G. Eda, C. Mattevi, H. Yamaguchi, H. Kim, M. Chhowalla, *J. Phys. Chem. C* **2009**, *113*, 15768.
[24] T. Q. Trung, N. T. Tien, D. Kim, J. H. Jung, O. J. Yoon, N.-E. Lee, *Adv. Mater.* **2012**, *24*, 5254.
[25] X. W. Fu, Z. M. Liao, J. X. Zhou, Y. B. Zhou, H. C. Wu, R. Zhang, G. Jing, J. Xu, X. Wu, W. Guo, D. Yu, *Appl. Phys. Lett.* **2011**, *99*, 213107.
[26] S. M. Choi, S. H. Jhi, Y. W. Son, *Phys. Rev. B* **2010**, *81*, 081407.
[27] S.-K. Lee, H. Y. Jang, S. Jang, E. Choi, B. H. Hong, J. Lee, S. Park, J.-H. Ahn, *Nano. Lett.* **2012**, *12*, 3472–3476.
[28] Q. He, S. Wu, S. Gao, X. Cao, Z. Yin, H. Li, P. Chen, H. Zhang, *ACS Nano* **2011**, *5*, 5038–5044.
[29] S. Pang, Y. Hernandez, X. Feng, K. Müllen, *Adv. Mater.* **2011**, *23*, 2779–2795.
[30] G. Eda, G. Fanchini, M. Chhowalla, *Nat. Nanotechnol.* **2008**, *3*, 270.
[31] W. H. Lee, J. Park, S. H. Sim, S. B. Jo, K. S. Kim, B. H. Hong, K. Cho, *Adv. Mater.* **2011**, *23*, 1752–1756.
[32] M.-S Lee, K. Lee, S.-Y. Kim, H. Lee, J. Park, K.-H. Choi, H.-K Kim, D.-G. Kim, D.-Y. Lee, S. W. Nam, J.-U. Park, *Nano Lett.* **2013**, *13*, 2814–2821.
[33] S.-K. Lee, B. J. Kim, H. Jang, S. C. Yoon, C. Lee, B. H. Hong, J. A. Rogers, J. H. Cho, J.-H. Ahn, *Nano Lett.* **2011**, *11*, 4642–4646.
[34] R.-H. Kim, M.-H. Bae, D. G. Kim, H. Cheng, B. H. Kim, D.-H. Kim, M. Li, J. Wu, F. Du, H.-S. Kim, S. Kim, D. Estrada, S. W. Hong, Y. Huang, E. Pop, J. A. Rogers, *Nano Lett.* **2011**, *11*, 3881–3886.
[35] H. Chang, Z. Sun, Q. Yuan, F. Ding, X. Tao, F. Yan, Z. Zheng, *Adv. Mater.* **2010**, *22*, 4872–4876.
[36] K. S. Novoselov, A. K. Geim, S. V. Morozov, D. Jiang, Y. Zhang, S. V. Dubonos, I. V. Grigorieva, A. A. Firsov, *Science* **2004**, *306*, 666.
[37] Q. He, H. G. Sudibya, Z. Yin, S. Wu, H. Li, F. Boey, W. Huang, P. Chen, H. Zhang, *ACS Nano* **2010**, *4*, 3201–3208.
[38] J. Yang, J.-W. Kim, H. S. Shin, *Adv. Mater.* **2012**, *24*, 2299–2303.
[39] G. Eda, M. Chhowalla, *Adv. Mater.* **2010**, *22*, 2392–2415.
[40] W. C. Shin, S. Seo, B. J. Cho, *Appl. Phys. Lett.* **2011**, *98*, 153505.
[41] S. Shang, W. Zeng, X. Tao, *J. Mater. Chem.* **2011**, *21*, 7274–7280.
[42] S. Sahoo, S. K. Barik, G. L. Sharma, G. Khurana, J. F. Scott, R. S. Katiyar, arXiv:1204.1928v1.
[43] Y. G. Seol, J. S. Park, N. T. Tien, N.-E. Lee, D. K. Lee, S. C. Lee, Y. J. Kim, C.-S. Lee, H. Kim, *J. Electrochem. Soc.* **2010**, *157*, H1046.
[44] Y. G. Seol, W. Heo, J. S. Park, N.-E. Lee, D. K. Lee, Y. J. Kim, *J. Electrochem. Soc.* **2011**, *158*, H931.
[45] S. Park, J. An, I. Jung, R. D. Piner, S. J. An, X. Li, A. Velamakanni, R. S. Ruoff, *Nano Lett.* **2009**, *9*, 1593–1597.
[46] S. Stankovich, R. D. Piner, S. T. Nguyen, R. S. Ruoff, *Carbon* **2006**, *44*, 3342–3347.